Volume 50 | Number 3 | 11 January 2014 | Pages 251–372

ChemComm

Chemical Communications

www.rsc.org/chemcomm

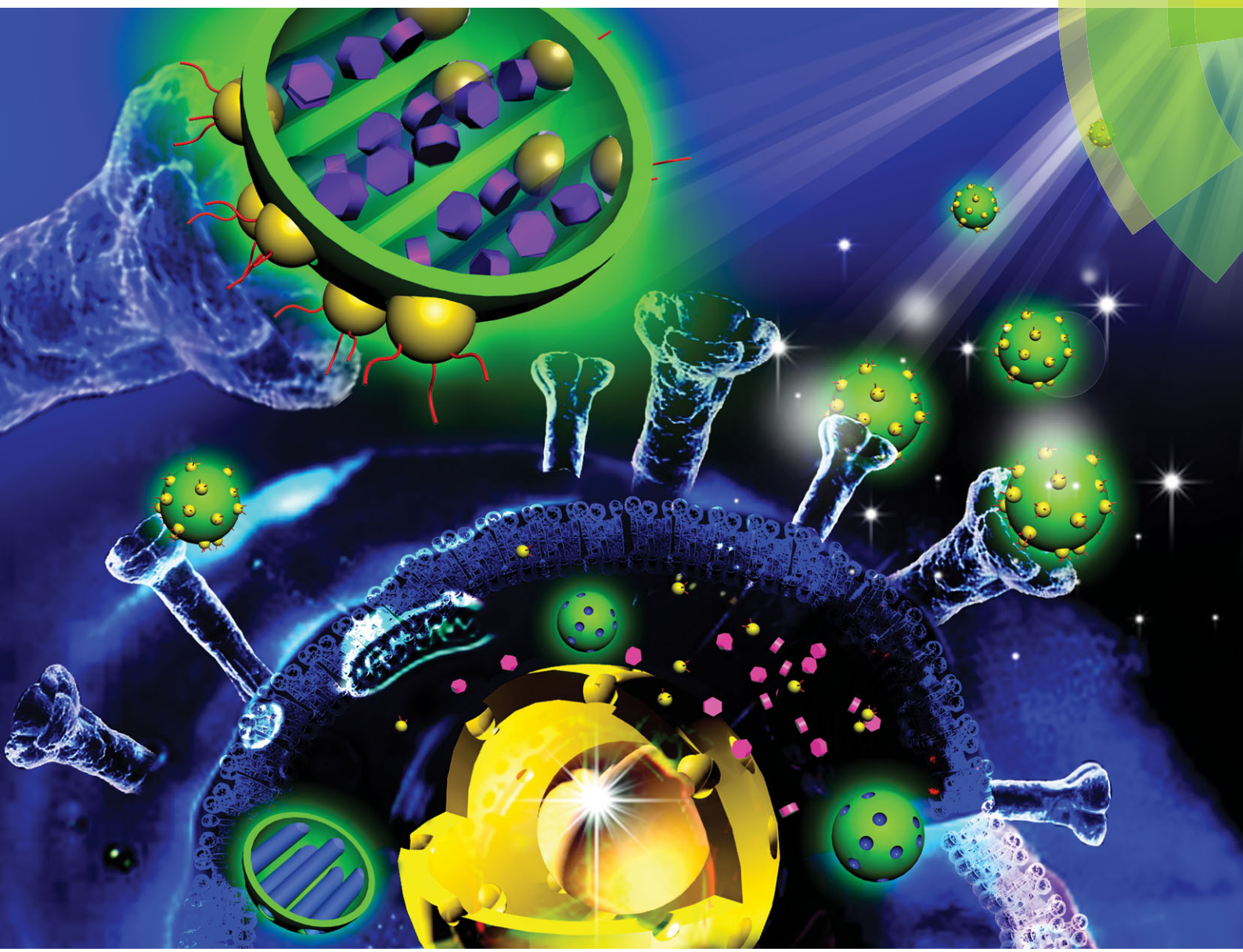

ISSN 1359-7345

ROYAL SOCIETY OF CHEMISTRY

COMMUNICATION

Xin Zhou *et al.*

pH-Triggered Au-fluorescent mesoporous silica nanoparticles for ^{19}F MR/fluorescent multimodal cancer cellular imaging

ChemComm

COMMUNICATION

pH-Triggered Au-fluorescent mesoporous silica nanoparticles for ^{19}F MR/fluorescent multimodal cancer cellular imaging†

Cite this: *Chem. Commun.*, 2014, 50, 283

Received 25th September 2013, Accepted 15th October 2013

DOI: 10.1039/c3cc47324d

www.rsc.org/chemcomm

Shizhen Chen, Yuqi Yang, Haidong Li, Xin Zhou* and Maili Liu

Novel pH-triggered nanoprobe were fabricated for ^{19}F MRI and fluorescence imaging (MRI-FI) of cancer cells. The biocompatibility, durability, high internalizing efficiency and pore architecture justify the Au-fluorescent mesoporous silica nanoparticles as ideal, highly sensitive and highly specific vectors for ^{19}F MRI and FI of cancer cells.

Conventional ^{1}H magnetic resonance imaging (MRI) or fluorescent imaging (FI) techniques for the detection of early-stage cancers are often limited by either low sensitivity or shallow penetration.[1,2] When integrating these two imaging modalities, one can take advantages of both to identify the cancer cells more accurately and robustly. Therefore, multimodal MR/fluorescent probes have attracted a lot of attention recently.[3] ^{1}H MRI is generally used as one such multimodal imaging, as protons widely exist in chemical molecules and biological tissues.[4] Due to the high natural abundance (99.99%) and large gyromagnetic ratio, protons give a much higher MRI signal in comparison to other nuclei. Nevertheless, for specific molecular imaging or cellular imaging, ^{1}H MRI sometimes could not generate high-contrast images because of the huge background signal produced in biological systems, like water.

However, there is almost no endogenous ^{19}F element in the cells and biological molecules that might be a source of background noise. Also, ^{19}F has 100% natural abundance and the sensitivity is slightly lower than that of ^{1}H even without any hyperpolarization.[5,6] Therefore, ^{19}F MRI has an extraordinary capability to achieve high-contrast images to light up the 'hot spots', which are very helpful in identifying or tracing tumor cells. A variety of stimuli-sensitive ^{19}F intracellular MR probes have been developed to date,[7] and ^{19}F cellular MRI has been accordingly considered as a kind of powerful and noninvasive methodology for cancer diagnosis.[8] A major key to the success of cancer diagnosis has been the development of nanosized and specific ^{19}F probes capable of complete on–off regulation of the ^{19}F MR signal in response to the tumor environment, which enables ^{19}F MRI to be performed after they are internalized into target cells.[9]

In recent years, the use of nanoparticles for biomedical imaging has revolutionized the monitoring of molecular and cellular events in living organisms.[10,11] Nanoparticle based controlled release systems have attracted great attention owing to their applicability in the field of drug delivery. A diverse range of organic carriers, including micelles, liposomes, and polymeric nanoparticles, has been investigated to be used as delivery systems.[12] However, organic carriers such as micelles suffer from poor stability due to biochemical attack. Among the range of available nanoparticles, mesoporous silica nanoparticles (MSNs) have attracted attention as a promising component in controlled release systems.[13]

The unique structural features of organically functionalized MSNs—such as their chemically and thermally stable mesoporous structure, large surface area, tunable pore size, and well-defined surface properties—make them ideal for hosting guest molecules of various sizes, shapes and functions.[14] MSNs are excellent candidates for many biomedical applications, owing to their straightforward synthesis and low-toxicity degradation pathways in the biological environment. They are promising vehicles for intracellular contrast agents, because they are capable of storing and releasing molecules on command. In particular, several recent reports have shown that MSNs can be efficiently endocytosed by mammalian cells.[15] Recently, multifunctional nanostructured materials have been applied for multimodal imaging and simultaneous diagnosis and therapy.[3] Therefore, we propose to synthesize fluorescein-functionalized mesoporous silica nanoparticles (FMSNs) as platforms for MR/fluorescent multimodal imaging, because they are highly stable in aqueous solution and have good fluorescent properties.

In the case of the FMSNs controlled release system, a variety of capping agents—including nanoparticles, organic molecules, and supramolecular nanovalves—have been employed as "gatekeepers" that can be manipulated using various stimuli, such as changes in pH, redox state, electrostatics, enzymatic activity, photo-irradiation, magnetic actuation, and electric field. Upon stimulation, these gatekeepers allow the release of cargo from the reservoir into a specific environment. As for the tumor microenvironment, it exhibits

Key Laboratory of Magnetic Resonance in Biological Systems, State Key Laboratory for Magnetic Resonance and Atomic and Molecular Physics, Wuhan Center for Magnetic Resonance, Wuhan Institute of Physics and Mathematics, Chinese Academy of Sciences, Wuhan 430071, China. E-mail: xinzhou@wipm.ac.cn

† Electronic supplementary information (ESI) available. See DOI: 10.1039/c3cc47324d

significant differences compared with normal tissues, because of the altered metabolic profile of malignancy. For example, cancer cells usually live in a more acidic environment than the normal tissue because of the resulting upregulated glycolytic metabolism, increased generation of lactic acid, and lowered cellular pH values due to tumorigenesis. Of the stimuli studied previously, the change in pH represents an effective strategy for cancer diagnosis.

Here, we designed and synthesized novel, nanosized and pH-triggered probes based on the encapsulation of the ^{19}F contrast agent in AuNP-capped FMSNs, called Au-FMSNs, for the intracellular ^{19}F MRI-FI. Functional AuNPs were employed to seal the nanopores in the FMSNs, in order to inhibit the premature release of the ^{19}F contrast agent. AuNPs were covalently conjugated onto the FMSNs by acid-cleavable hydrazone linkages. At neutral pH (pH 7.4), the hydrazone linkers remain intact and pores are blocked with AuNPs in order to prevent the ^{19}F MR contrast agent from diffusing out of the pores. At acidic pH (pH $<$ 6.0), the hydrazone linkers are cleaved and thus the gold caps are removed, allowing the release of the entrapped contrast agent from such a pH-triggered Au-FMSN platform. Folate has been covalently conjugated to AuNPs *via* the formation of amide bonds for targeting the cancer cells, because folate-binding proteins (FBP) are selectively overexpressed on the membranes of cancer cells (Scheme 1A). For the normal cells with neutral pH, the ^{19}F MRI is 'dark' as the ^{19}F contrast agent is trapped in the Au-FMSNs, and the FI confirms that the Au-FMSNs are outside the cell membrane. However, for the cancer cells with acidic pH, the folate-functional Au-FMSNs are able to enter the cancer cells. The hydrazone bonds are cleaved in the intracellular acidic environment (pH 5–6), resulting in 'light on' of the ^{19}F intracellular MRI due to the release of the ^{19}F contrast agent from the FMSNs, and the FI also demonstrates that the Au-FMSNs are endocytosed by the cancer cells (Scheme 1B).

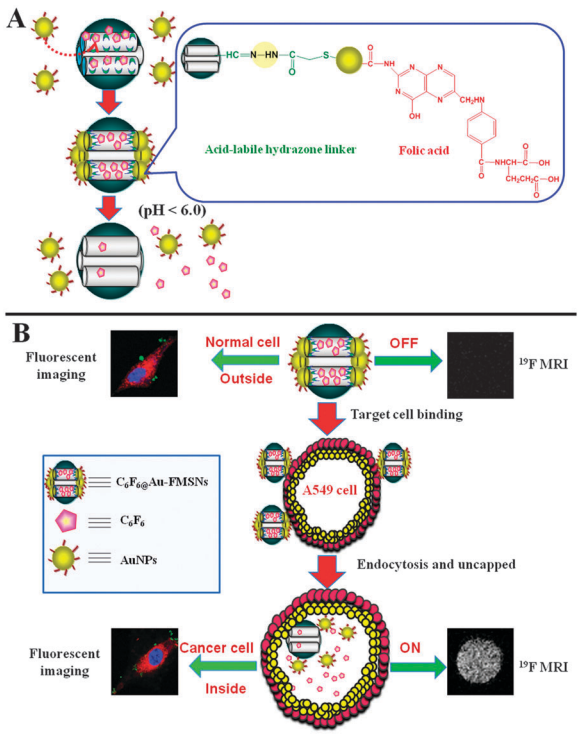

Scheme 1 (A) The synthesis procedure of AuNPs capped FMSNs. Folic acid with a high tumor affinity was conjugated onto the surface of the AuNPs, due to the overexpression of its receptors on the cancer cells, AuNPs were covalently conjugated onto the FMSNs *via* acid-labile hydrazone linkers. (B) The pH-triggered release of the ^{19}F contrast agent from the Au-FMSNs to the cytosol *via* the selective removal of the AuNP cap in the acidic intracellular compartments of cancer cells.

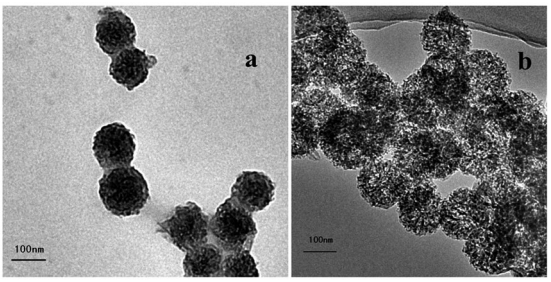

Fig. 1 TEM micrographs of (a) bare Au-FMSNs, and (b) Au-FMSNs after incubation in pH 6.0 PBS, showing the uncapping process of the AuNPs in the acidic environment.

The occurrence of the uncapping process between the FMSNs and AuNPs was confirmed using transmission electron microscopy (TEM), as shown in Fig. 1. In the case of the Au-FMSNs, distinctive, dark, crystalline spots with diameters of 4–5 nm were observed on the surfaces of the FMSNs (Fig. 1a). These AuNPs (4–5 nm in diameter) were large enough to block the 3.1 nm pores of the FMSNs, and thus inhibited the release of the loaded contrast agent. In contrast, when the Au-FMSNs were incubated in a pH 6.0 buffer solution, Au-uncapped FMSN particles were observed, as shown in Fig. 1b. The resulting spherical FMSNs had diameters of $\sim$100 nm, and 3.1 nm-wide channel-like pores, and the nanoparticles were all well dispersed and separated from one another.

To gain a better understanding of the uncapping process, the surface hydrophilicity of the FMSNs, Au-FMSNs and Au-FMSNs after being incubated in the pH 6.0 PBS for 60 min was characterized, respectively (Fig. S1, ESI†). X-ray photoelectron spectroscopy (XPS) was performed to analyze the resulting FMSNs and Au-FMSNs, as shown in Fig. S2 (ESI†). These results further confirmed the successful AuNP capping of the FMSNs. The average pore diameter was 3.1 nm, calculated using the Barrett–Joyner–Halenda (BJH) method, as shown in Fig. S3 (ESI†). The results indicated that the FMSNs were highly porous and had a large surface area, and also demonstrated that AuNPs efficiently blocked the pores of the FMSNs, which enabled them to encapsulate and deliver large quantities of ^{19}F contrast agents.

It is well known that the membranes of human lung cancer cells (A549) have many folate receptors. The folate groups on the Au-FMSNs could also play a dominant role in facilitating receptor-mediated endocytosis. To evaluate the efficiency and pathway of specific cellular uptake for folate functionalized Au-FMSNs, we stained the nuclei of the cells with DAPI (blue) and the cell membrane with DiI (red), and monitored the Au-FMSNs (green) incubated for different times in 100 μg mL^{-1} solutions of human lung cancer cells (A549) and normal human lung fibroblast cells (MRC-5) by confocal fluorescence microscopy (CLSM). The cellular uptake and subsequent localization of the Au-FMSNs is shown in Fig. 2; the green fluorescent spots represent the

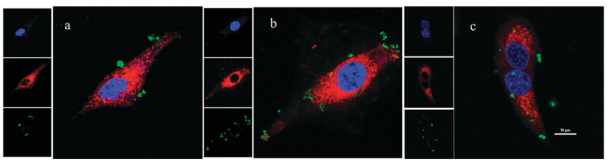

Fig. 2 Fluorescence confocal micrographs of Au-FMSNs incubated in (a) normal human lung fibroblast cells (MRC-5) for 3 h, (b) human lung cancer cells (A549) for 30 min, and (c) A549 cells for 3 h. Nucleus is stained in blue, cell membrane is stained in red, Au-FMSNs are shown as green spots. It shows that Au-FMSNs can be selectively endocytosed by lung cancer cells (A549).

Au-FMSNs. It can be seen from Fig. 2a that after 3 h of incubation, almost all of the folate-functionalized Au-FMSNs were outside the MRC-5 cells. The green fluorescent spots shown in Fig. 2b indicate the folate-functionalized Au-FMSNs conjugated with the folate receptors, which were overexpressed in the membranes of the A549 cells. After 30 min of incubation, some of the Au-FMSNs adhered onto the cell membranes, and the rest of the Au-FMSNs were trapped inside the vesicles. In Fig. 2c the 100 nm Au-FMSNs could be clearly seen in both the cytoplasm and the nuclei of the A549 cells after 3 h of incubation. The observed luminescence was therefore attributed to the capability of our Au-FMSN system to encapsulate intracellular contrast agents.

After incubating C_6F_6@Au-FMSNs with pH 7.4 PBS, human lung cancer cells (A549) and pH 6.0 PBS for 60 min, the values of ^{19}F longitudinal relaxation time (T_1) measured by nuclear magnetic resonance (NMR) spectroscopy were estimated to be 3.2 s, 2.4 s and 1.8 s, respectively. The uncapped AuNPs from the FMSNs, *via* the cleavage of hydrazone linkages in the mildly acidic environment, induced the release of the ^{19}F contrast agent, and ^{19}F molecules entered into A549 cells and the solution of pH 6.0 PBS, shortening the T_1 due to the larger interaction in comparison to the ^{19}F trapped in the Au-FMSNs. In order to get a better ^{19}F MRI contrast of these three different incubated samples (as shown in Fig. 3), a repetition time (TR) of 3 s was chosen. For the incubation in pH 7.4 PBS, the pH-triggered ^{19}F biosensors were not activated, thereby exhibiting a dark signal (Fig. 3a). However, after 60 min of incubation in A549 cells, the AuNP lids became uncapped; this was in response to the extracellular pH of the tumor tissues, where the pH was 0.4–1.0 units lower than the general physiological pH (pH 7.4). An appreciably enhanced ^{19}F MRI signal was thus achieved in the intracellular pH environment of cancer cells due to the shorter T_1 (Fig. 3b). In pH 6.0 PBS, the AuNPs in the Au-FMSNs dissolved rapidly (Fig. 3c) and the T_1 of ^{19}F molecules was much shortened, resulting in a further enhancement of the ^{19}F MRI signal.

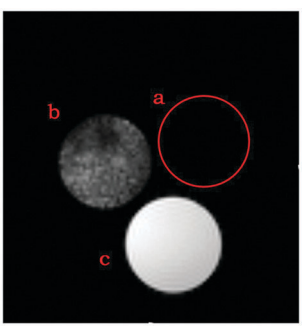

Fig. 3 ^{19}F MRI of C_6F_6@Au-FMSNs in (a) pH 7.4 PBS, (b) A549 lung cancer cells, (c) pH 6.0 PBS, where incubation was performed for 60 min. FOV (field of view) = 33 × 33 mm^2.

In order to investigate the time dependence of the uncapping dynamics of pH-triggered ^{19}F biosensors in the cancer cells, the C_6F_6@Au-FMSNs were incubated in A549 cancer cells at 37 °C for different times. Fig. S5 (ESI†) shows the ^{19}F intracellular MRI after incubation for different times. The longer the incubation time, the stronger the MRI signal, due to the shorter T_1 of ^{19}F in cancer cells compared with that in Au-FMSNs. For more than 120 min of incubation, the MRI signal almost approached a steady state, which indicated that the uncapping of Au-FMSNs had reached equilibrium.

We have designed and synthesized the Au-FMSNs platform based nanoprobes, which can be used for MRI and fluorescent multimodal imaging. Fluorescent imaging reveals the highly selective uptake of these nanoprobes by A549 cancer cells, and that the Au lids were efficiently uncapped in the acidic intracellular compartments of cancer cells. It induced the release of the ^{19}F MRI contrast agent from the pores of the FMSNs into the cytosol, appreciably enhancing the intracellular ^{19}F MRI signal. These nanoprobes have great potential to be utilized as high-sensitivity MRI and fluorescent multimodal biosensors for tumors, and the Au-FMSN platform could also be applied in the field of either contrast agents or drug delivery.

This work was supported by the Natural Science Foundation of China (81227902, 21221064, 21120102038, 11004228, 21305156), the Innovation Method Fund of China (2010IM030600), and the Chinese Academy of Sciences (the 100 talents program & KJCX2-EW-N06-04).

Notes and references

1 A. H. Fu, R. J. Wilson, B. R. Smith, J. Mullenix, C. Earhart, D. Akin, S. Guccione, S. X. Wang and S. S. Gambhir, *ACS Nano*, 2012, **6**, 6862–6869.
2 J. Liu, W. Zhang, H. Zhang, Z. Yang, T. Li, B. Wang, X. Huo, R. Wang and H. Chen, *Chem. Commun.*, 2013, **49**, 4938–4940.
3 A. Louie, *Chem. Rev.*, 2010, **12**, 3146–3195.
4 R. J. Perrin, A. M. Fagan and D. M. Holtzman, *Nature*, 2009, **461**, 916–922.
5 X. Zhou, D. Graziani and A. Pines, *Proc. Natl. Acad. Sci. U. S. A.*, 2009, **40**, 16903–16906.
6 M. Boccalon, P. Franchi, M. Lucarini, J. J. Delgado, F. Sousa, F. Stellacci, I. Zucca, A. Scotti, R. Spreafico, P. Pengo and L. Pasquato, *Chem. Commun.*, 2013, **49**, 8794–8796.
7 K. Kikuchi, *Chem. Soc. Rev.*, 2010, **39**, 2048–2053.
8 J. J. Liu, R. Horst, V. Katritch, R. C. Stevens and K. Wüthrich, *Science*, 2012, **335**, 1106–1110.
9 Y. Takaoka, T. Sakamoto, S. Tsukiji, M. Narazaki, T. Matsuda, H. Tochio, M. Shirakawa and I. Hamachi, *Nat. Chem.*, 2009, **1**, 557–561.
10 K. Kohara, S. Yamamoto, L. Seinberg, T. Murakami, M. Tsujimoto, T. Ogawa, H. Kurata, H. Kageyama and M. Takano, *Chem. Commun.*, 2013, **49**, 2563–2565.
11 A. Lesniak, A. Salvati, M. J. Santos-Martinez, M. W. Radomski, K. A. Dawson and C. Aberg, *J. Am. Chem. Soc.*, 2013, **135**, 1438–1444.
12 D. Peer, J. M. Karp, S. Hong, O. C. Farokhzad, R. Margalit and R. Langer, *Nat. Nanotechnol.*, 2007, **2**, 751–760.
13 A. T. Dickschat, F. Behrends, S. Surmiak, M. Weiß, H. Eckert and A. Studer, *Chem. Commun.*, 2013, **49**, 2195–2197.
14 Z. X. Li, J. C. Barnes, A. Bosoy, J. Stoddart and J. I. Zink, *Chem. Soc. Rev.*, 2012, **41**, 2590–2605.
15 F. Torney, B. G. Trewyn, V. S. Y. Lin and K. Wang, *Nat. Nanotechnol.*, 2007, **2**, 295–300.